CRYSTAL GROWTH & DESIGN

Article

Cite This: Cryst. Growth Des. 2017, 17, 4151-4161

pubs.acs.org/crystal

Influence of Solvent Composition on the Crystal Morphology and Structure of *p*-Aminobenzoic Acid Crystallized from Mixed Ethanol and Nitromethane Solutions

Published as part of a Crystal Growth and Design virtual special issue of selected papers presented at the 12th International Workshop on the Crystal Growth of Organic Materials (CGOM12 Leeds, UK)

I. Rosbottom,*[,†] C. Y. Ma,[†] T. D. Turner,[†] R. A. O'Connell,[†] J. Loughrey,[‡] G. Sadiq,[§,#] R. J. Davey,[§] and K. J. Roberts[†]

[†]Centre for the Digital Design of Drug Products, School of Chemical and Process Engineering and [‡]School of Chemistry, University of Leeds, Leeds LS2 9JT, U.K.

[§]School of Chemical Engineering and Analytical Science, University of Manchester, Manchester M13 9PL, U.K.

Supporting Information

ABSTRACT: The crystallization of α-*p*-aminobenzoic acid (*p*ABA) from mixed solutions in ethanol (EtOH) and nitromethane (NMe) is reported. From solutions with compositions >60 wt % NMe, the known α-polymorph of *p*ABA appears. In contrast, crystals prepared from mixed solvent with <60 wt % NMe reveal the presence of a previously unknown NMe solvate, which crystallizes concomitantly with the α-form. The crystal structure of this new form has been determined and is compared with the previously known structure of the α-polymorph. The crystal structure of the NMe solvate has similar synthonic interactions with respect to α-*p*ABA, in particular, the OH···O H-bonded dimers and the NH···O H-bonds between the *p*ABA molecules. However, the π−π stacking interactions between the phenyl ring groups are found to be much more offset and do not form a continuous chain through the structure, as found in α-*p*ABA. The synthonic interactions in the NMe solvate structure are generally weaker than those found in α-*p*ABA, and the lattice energy is calculated to be significantly lower, suggesting the solvate structure is metastable with respect to α-*p*ABA. The impact of NMe on the morphology of α-pABA crystals, together with molecular modelling results suggest that this solvent is able to disrupt the π−π stacking interactions that dominate growth along the needle (*b*-axis) direction of α-pABA, and are intimately linked to the ultimate formation of the solvate.

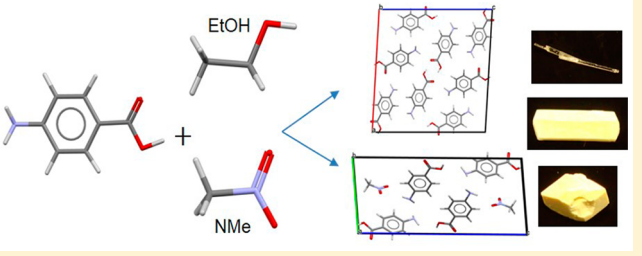

1. INTRODUCTION

The demand for active pharmaceutical ingredients (APIs) to be crystallized with high purity and desirable physical properties for downstream unit processes has resulted in increased importance being attributed to the crystallization solvent selection process. This is in order to quantify the impact of changes in solvent composition on the physical characteristics of the crystalline product, such as propensity to form solvates[1−5] and variations in crystal morphology.[6−13] Since a third of materials are known to produce solvates,[14] a detailed understanding of polymorphism and solvate formation can be vital in terms of consistent production of pure and stable drug products. As a caveat to this, avoiding needle-like morphologies is also important in pharmaceutical and fine chemical product processing, since they can create problems in downstream processing with their propensity to block filters and pipes, along with their undesirable mechanical properties that can result in their breakage during filtration.[15] Therefore, there is a need to correlate these material properties with molecular and crystal structural packing features,[1,2,16−18] to design highly pure crystalline particles with pre-defined physical properties.

Solvent screening can be a key step to assess the crystal form and morphology of APIs produced from solution,[19] in order to ensure the stability of a drug product and avoid product failure, resulting in the expensive process of product withdrawal and reformulation.[20] Experimental screening can be expensive and time-consuming; hence computational modeling can be used to guide the solvent selection process for API crystallization.[2,4,5,17,21−29] Once a stable solid form has been confirmed, the crystallization of this form with an isotropic crystal morphology can often be desirable. Though the crystallization of more isotropic morphologies can sometimes be achieved through control of the solute concentration (supersaturation) during solution crystallization,[30−32] it can also be achieved by

Received: March 24, 2017
Revised: June 15, 2017
Published: June 27, 2017

DOI: 10.1021/acs.cgd.7b00425
Cryst. Growth Des. 2017, 17, 4151−4161

manipulating the solvent composition.[33−35] Previous studies have demonstrated that an understanding of the individual crystal surface chemistry, solvent physical properties, and solution supersaturation can result in more effective solvent or additive selection/design for tailoring the crystal growth and morphology.[36−39] Therefore, the ability to design crystallization processes via solvent selection and/or other control techniques is of significant importance to produce a stable solid form and desirable crystalline physical properties.

Crystallizing from a mixture of solvents with different properties can effectively alter the physical properties (morphology, purity, crystallinity, etc.) of a material.[34,35,40] Cook et al.[41] observed that the mixture of a strong hydrogen bond (H-bond) donor and a strong H-bond acceptor can cause the deviation of the solution properties from regular solution theory.[42] Additionally, Chen et al.[9] demonstrated the applicability of using a computational approach to the design of a mixed solvation environment that modified the needle-like morphology of 2,6-dihydroxy-benzoic acid. Such studies have identified that understanding a solution crystallization environment on the molecular level can aid in rationalizing the solution behavior and physical properties of the crystals produced.

Drawing upon the above ideas, this study addresses the issue of solvent selection in the crystallization of *p*-aminobenzoic acid (*p*ABA), demonstrating first how the Cambridge Structural Database (CSD) may be used as a tool for directing solvent choice, and second how state-of-the-art synthonic engineering tools[17,43,44] may be used to aid our understanding of how solvents control both the morphology and phase of resulting solid forms. It is now well-known that the α and β polymorphs of *p*ABA are enantiotropically related, having a transition temperature of ∼14 °C.[45,46] It has also been reported that only needle-like crystals of the high temperature stable α form appear from organic solvents (e.g., alcohols, ethyl acetate, acetonitrile) regardless of the temperature.[47,48] The more prismatic β-*p*ABA has only been found so far to crystallize from water.[17,47,49,50] The search for a new solvent was thus initially motivated by the desire to crystallize the β polymorph directly from an organic solvent. As described below, this search led to the use of nitromethane (NMe) and nitromethane/ethanol mixtures as the crystallization media[49] and, ultimately, to examine the solvent effect on crystalline phase and morphology. The results are rationalized using molecular and synthonic modeling of the solvent interaction with both *p*ABA molecules and crystal surfaces of α-*p*ABA, in an attempt to understand at the molecular level, the observed crystalline structural form and morphology produced from the different solvent mixtures.

2. MATERIALS AND METHODS

2.1. Materials. Ethanol was purchased from VWR chemicals having a purity of 99.9% (CAS: 64-17-5). Nitromethane with >99% purity was purchased from ACROS Organics (CAS: 75-52-5). The *p*ABA was purchased from Sigma-Aldrich with 99% purity (CAS: 150-13-0).

2.2. Experimental Methods. *2.2.1. Solubility Determination.* Saturated solutions of α-*p*ABA in pure EtOH and EtOH/NMe mixtures (NMe concentration was increased in 10 wt % steps all the way up to pure NMe) were prepared at the 10 mL scale, agitated at the desired temperature for 24 h, and allowed to settle for 12 h, when the supernatant was pipetted into a fresh sample vial and dried. The mass of solid was weighed using a four-figure balance, and the mass was checked over 3 days to ensure all solvent had evaporated.

2.2.2. van't Hoff Solubility Analysis. If a solution is assumed to be ideal, that is, the solute/solute, solute/solvent, and solvent/solvent interactions are all equal, then the ideal solid/liquid equilibrium can be expressed, assuming a negligible contribution from the heat capacity, as eq 1

$$\ln(x) = \frac{\Delta H_{\text{fus}}}{R}\left[\frac{1}{T} - \frac{1}{T_{\text{m}}}\right] \tag{1}$$

where R is the ideal gas constant, ΔH_{fus} is the enthalpy of fusion, T is the temperature, and T_{m} is the melting temperature of α-*p*ABA.[51] However, since most solutions are nonideal, the van't Hoff equation can be used to assess the degree of nonideality, shown in eq 2

$$\ln(x) = -\frac{\Delta H_{\text{diss}}}{RT} + \frac{\Delta S_{\text{diss}}}{R} \tag{2}$$

where ΔH_{diss} and ΔS_{diss} are the enthalpy and entropy of dissolution, respectively. Since R, T, ΔH_{diss} and ΔS_{diss} are constants, the solubility can be plotted as $\ln(x)$ vs $\frac{1}{T}$. Solubility plotted in van't Hoff coordinates that is found to be above the ideal line implies that the solute/solvent interactions are stronger than the solvent/solvent interactions. Conversely, if the solubility is found to be below the ideal line, this then implies that the solvent/solvent interactions are stronger than the solute/solvent interactions. A more in-depth derivation and analysis of this theory can be found in a previous publication.[52]

2.2.3. Crystallization Screening. The crystals were obtained from cooling crystallization in EtOH/NMe solvent mixtures of 0% (by weight) to 100% NMe content, at two supersaturations of S = 1.1 and S = 1.3. Ten grams of solvent with the appropriate amount of α-*p*ABA was agitated at 50 °C using a Julabo[53] F25 circulator for an hour to ensure full dissolution of the solid. Then the agitation was halted and the solutions were cooled to 10 °C and left to crystallize, whereby crystallization occurred within 5 days. Solutions were vacuum filtered to isolate the solid crystalline form from the solution.

Crystals of the pure nitromethane solvate were prepared using slow solvent evaporation. Five milliliters of pure nitromethane was saturated with α-*p*ABA at ambient temperature and pressure; this was then filtered into a clean 10 mL screw cap vial and covered using plastic paraffin film with a single hole punctured through using a clean needle. The solvent was allowed to evaporate slowly over 3 days; the resulting crystals were isolated using vacuum filtration and air-dried.

2.2.4. Crystal Morphology Characterization. The crystals obtained were imaged by high quality photography using an Olympus Style TG4 camera.

2.2.5. Structural Characterization. Powder X-ray diffraction (PXRD) of the samples was carried out using a Bruker D8 advanced X-ray diffractometer, which used Cu Kα radiation and a germanium primary monochromator in a Bragg−Brentano reflection geometry. The step size used was 0.033 2θ, with a step time of 180 s/step over a 2θ range of 5−39.8° 2θ. The detector used was a Vantec-1 position sensitive detector. Samples were prepared by grinding crystallization products in a mortar and pestle and mounting on a flat plate sample holder. Data reduction and Rietveld analysis were performed using PANanalytical Highscore plus software.[54]

For single X-ray diffraction, crystals were immersed in inert oil and mounted on a nylon loop. These were then cooled to 100 K using an Oxford Cryosystems 700 Series Crysostream Cooler[55] and data collected on a RigakuSuperNova diffractometer fitted with an Atlas CCD detector with monochromated Mo−Kα radiation (λ = 0.71073 Å). The data set was collected and processed using CrysAlisPRO[56] and corrected for absorption using an analytical numeric correction;[57] the structure was solved using SHELXS[58] and refined by full-matrix least-squares on F^2 using ShelXL-2014[59] interfaced through the program Olex2.[60] Molecular graphics and tables of data were produced using Olex2.[60] All non-hydrogen atoms were located in the Fourier Map and refined anisotropically. All hydrogen atoms bound to carbon were placed in calculated positions and refined isotropically using a "riding model".

2.3. Computational Methods. *2.3.1. Synthon Characterization.* The strength and nature of the intermolecular interactions in the bulk crystal structure (intrinsic synthons) were characterized using

DOI: 10.1021/acs.cgd.7b00425
Cryst. Growth Des. 2017, 17, 4151−4161

HABIT98.[61] A nest of unit cells were constructed in three dimensions, and the interactions between a molecule in the central unit cell and all of the other molecules in the surrounding unit cells were calculated. The atom−atom parameters published by Momany et al.[62] together with fractional charges calculated using the AM1 method within MOPAC[63,64] were used to calculate the strength of the intermolecular interactions in this study. This method for calculating synthon strength has been widely used in the molecular modeling of organic materials.[17,63,65−68]

2.3.2. Molecular and Surface Grid-Based Searching. The most favored binding sites between the solute and solvents were identified using the systematic search program.[69−71] The program operates with a stationary and mobile phase, and in this case they can be single molecules and dimers and hence simply be referred to as a "body". The stationary body is fixed, while the mobile body moves around the stationary body on a grid. At each grid point, the mobile phase can also rotate about three angles. At each point and rotation, the intermolecular energy was calculated using the same potential parameters mentioned in Section 2.3.2.

In this study, the most favored binding sites of up to five molecules of NMe and ethanol with a *p*ABA dimer were identified. The binding sites were searched sequentially. For the first simulation, the *p*ABA dimer was held rigid, and the solvent molecule was moved around the grid surrounding the dimer, and the most favorable interaction between a solvent molecule and the dimer was identified. The coordinates for the most favored interaction between the *p*ABA dimer and one solvent molecule was used as the starting point for the second simulation, where it was held rigid, and a second solvent molecule was searched in the same way as the first simulation to find the most favored binding site of a second solvent molecule. This search procedure was repeated for up to five molecules of the solvent.

For the surface searching,[72,73] a crystal surface, represented by a slab, was generated and the slab was then treated as a fixed body during the searching process. The thickness of the slab was selected to be a multiple of the *d*-spacing (d_{hkl}) between adjacent (*hkl*) lattice planes, while the surface area was a multiple of the crystal unit cell sizes. Therefore, the surface is embedded in an $n_1 \times n_2 \times n_3$ matrix to eliminate the edge effects on the search results. The grid cells were generated based on three orientations of the mobile body and two spherical polar angles between the two bodies, but only covering half of the space facing the crystal surface, i.e., the azimuthal angle from 0 to 180°. The search explored every grid point and calculated the interaction energy between the slab and the mobile body (a probe molecule or cluster), and hence identified the most favorable sites for the mobile body to dock on or interact with the slab surface.

3. RESULTS AND DISCUSSION

3.1. Solvent Selection Application of the Cambridge Structural Database. A starting point in this study was a search of the CSD, with the objective of identifying molecular functionalities that could preferentially interact with the acid group of *p*ABA. Accordingly the CSD was searched for all crystal structures containing the *p*ABA moiety. Excluding the 6 entries for pure *p*ABA and the structures in which *p*ABA adopted the acid dimer, this amounted to 42 hits in which the acid hydroxyl was bound to a non *p*ABA group. Of these, 29 involved H-bonds directly to a nitrogen (as pyridine, bipyridine, imidazole), and 13 were bound to oxygen either as carbonyl (6), water (2), or nitro (5) functionality. On this basis, it was surmised that nitromethane would be an interesting solvent to explore since it had not previously been chosen for crystallization experiments. To our knowledge, this is the first report of the application of the CSD in solvent selection.

3.2. Solubility. Figure 1 shows the solubility measured in pure EtOH, NMe, and in mixtures of EtOH/NMe in steps of 10% by weight in the temperature range 10−30 °C.

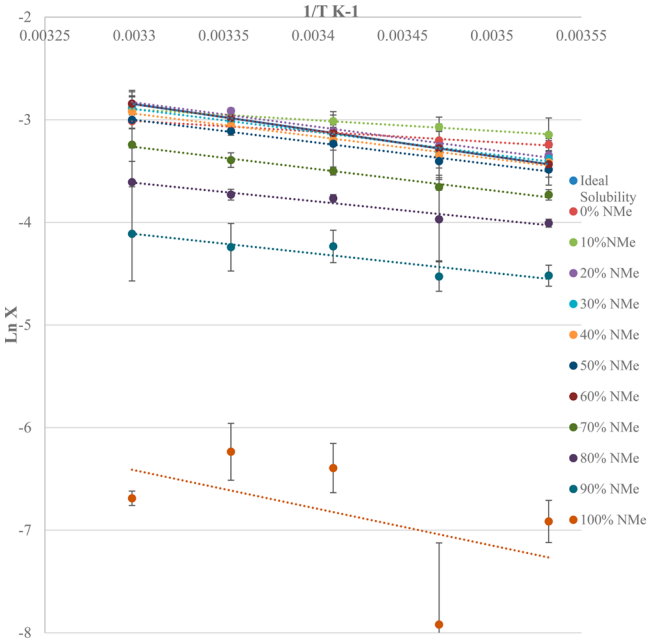

Figure 1. Solubility for the different solvent compositions plotted using the van't Hoff relationship with the ideal solubility (eq 1) indicated by the solid black line.

The data in Figure 1 shows that only the solubility up to about 30% NMe content was above the ideal solubility line, consistent with the increase in solubility seen upon addition of small amounts of NMe (Figure S1a, Supporting Information). It was also observed that the solubility at lower temperatures was further above the ideal solubility than at higher temperatures, which suggests that these liquids can be significantly undercooled and remain stable.[52] The large errors observed for the van't Hoff coordinates for pure NMe were due to the small amount of material produced from the solubility experiments; hence when measuring the mass of the material, any small deviation in the mass was translated into a large percentage error.

3.3. Crystallization from EtOH/NMe Mixtures. Cooling crystallization experiments yielded crystalline particles from all the solutions except pure nitromethane, where after 5 days no crystalline material could be obtained. The comparison of the PXRD spectra of the crystals produced at 10 °C from the solutions containing 10%, 30%, 50%, and 80% NMe is shown in Figure 2.

The crystals produced from the 90:10 EtOH/NMe sample displayed peaks that were consistent with the α-*p*ABA pattern, along with some prominent peaks not present in the α-*p*ABA pattern (labeled "new diffraction peaks" in Figure 2). These previously unseen peaks, consistent with the crystallization of a mixture of phases, were also observed in the 30:70 and 50:50 diffraction patterns, albeit at much lower intensities than in the 90:10 pattern. However, the 20:80 pattern showed no evidence of these previously unseen peaks.

A single crystal formed from cooling crystallization of a highly supersaturated solution of pure NMe was isolated and subject to single crystal X-ray diffraction (XRD). This revealed (see section 3.4) that a *p*ABA/NMe solvate structure had been formed. The calculated PXRD pattern based on this solvate was consistent with, and hence explained, the previously unseen peaks found in some of the PXRD patterns from the mixed solutions that were due to concomitant crystallization of the

DOI: 10.1021/acs.cgd.7b00425
Cryst. Growth Des. 2017, 17, 4151−4161

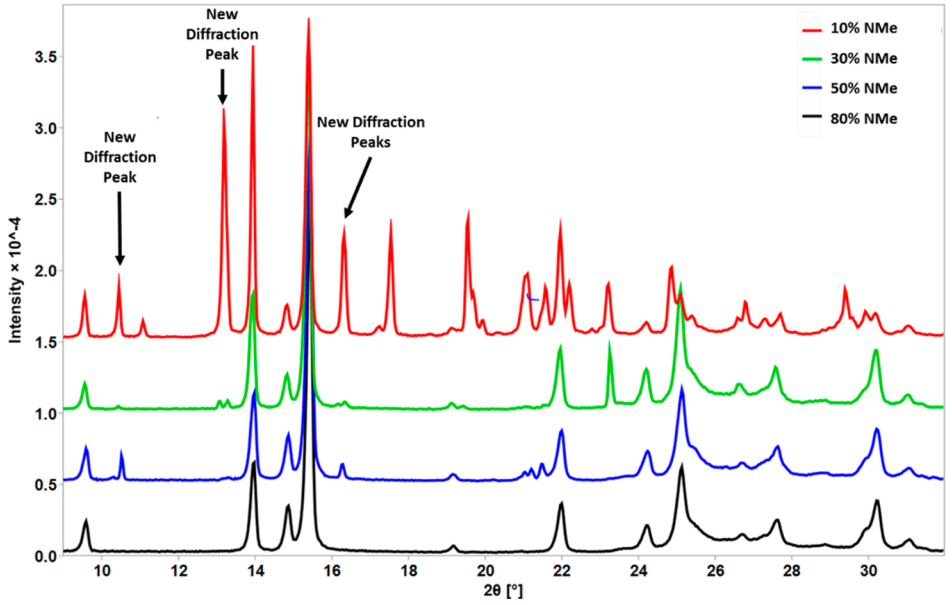

Figure 2. Comparison of the PXRD spectra of the crystals produced from the solution containing 10% NMe (red); 30% NMe (green); 50% NMe (blue); and 80% NMe (black). New peaks labeled are peaks not consistent with *α*-*p*ABA structure.

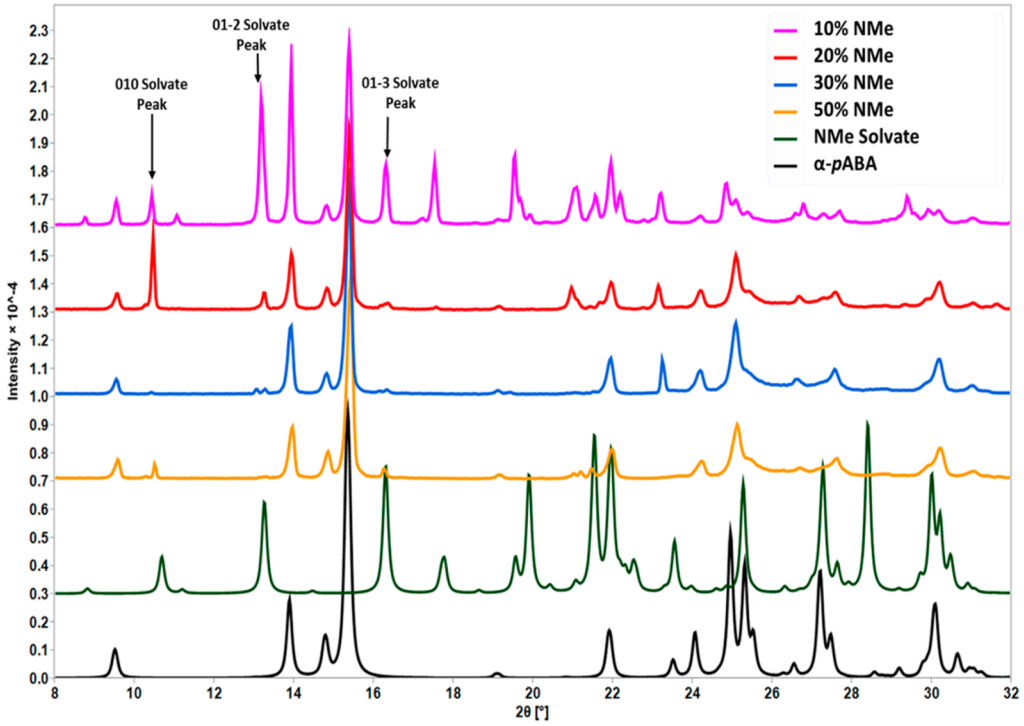

Figure 3. Overlay of experimental diffraction patterns for the 10, 20, 30, and 50% NMe samples, which contained peaks related to the solvate phase, with a comparison to the simulated diffraction patterns of the NMe solvate and *α*-*p*ABA structure files.

Table 1. Weight Percentage Values of the Solvate in the Samples Containing Solvate Peaks, Together with the Goodness of Fit of the Rietveld Refinement

sample	100% NMe[a]	90% NMe	80% NMe	70% NMe	60% NMe	50% NMe	40% NMe	30% NMe	20% NMe	10% NMe
solvate weight %	100	0	0	0	0	9.0	0	3.6	27.7	80.1
RWP of refined structures	N/A	N/A	N/A	N/A	N/A	27.8	N/A	27.8	41.6	41.2

[a]Solution did not crystallize over 5 days using the method described in section 2.2.3; hence, the production of the pure NMe solid was achieved using slow solvent evaporation in pure NMe.

NMe solvate and *α*-*p*ABA phases (Figure 2). Figure 3 shows the comparison of calculated PXRD patterns of the NMe

DOI: 10.1021/acs.cgd.7b00425
Cryst. Growth Des. 2017, 17, 4151−4161

solvate and α-*p*ABA structures, with the PXRD patterns from the crystals produced from solutions containing 10%, 20%, 30%, and 50% NMe content.

Figure 3 shows that the "new peaks" from Figure 2 can be attributed to the 010, $01\bar{2}$, and $01\bar{3}$ peaks of the solvate crystal structure. The quantity of the solvate in each sample was calculated by full pattern Rietveld analysis, with pattern fitting to both the α-*p*ABA and the solvate structure files.

Table 1 shows that, in general, the amount of solvate present in the samples is reduced with increasing NMe content, with a maximum 80.1% of the solvate in the 10% NMe sample. It was observed that the samples with 40% and 70−90% NMe content contained no evidence of the solvate structure. It was also observed that the time taken to crystallize the solid increased with increasing NMe content in the solution. Therefore, this suggests that the decrease in the amount of solvate structure with increasing NMe content could be consistent with a metastability of the solvate structure, i.e., with increased induction time to crystallization resulting in the more stable α-*p*ABA structure. If the solvate phase was the more stable phase, it would be expected that the increase of NMe content would enhance the crystallization of the solvate phase. However, the fact that the solvent composition would impact on the transition temperature between the two phases must also be considered. From the data collected it seems likely that the α-phase is more stable than the solvate phase, and that nitromethane impacts the relative crystallization rates of the two forms.

However, it should be highlighted that the 100% NMe sample included in Table 1 was produced from a slow solvent evaporation experiment in pure NMe, which yielded a solid of the pure NMe solvate and a separate solid which was a mixture of α-*p*ABA and the NMe solvate. This therefore suggests that it takes extremely careful control over the crystallization conditions to produce a sample of the pure NMe solvate structure.

It should also be mentioned that for the solubility measurements given in Figure 1, the solid phase that was harvested from the supernatant was assumed to be α-*p*ABA. However, it has now been shown in Figures 2 and 3, along with Table 1, that a mixture of the α−*p*ABA and NMe solvate phases can be obtained from the cooling crystallization experiments in the EtOH/NMe solvent mixtures. Therefore, it must be stated that the solubility measurements quoted here could be influenced by the conversion of any of the material to the NMe solvate and that the solubility of this form is currently unknown. Hence, a future study that further examines the crystalline phase obtained from the gravimetric analysis solubility measurements, along with identifying the solubility of the solvate phase, could be of interest.

3.4. Solvate Crystal Structure and Chemistry. The unit cell and packing of the solvate crystal structure is shown in Figure 4.

Figure 4a shows that the solvent molecule with 54% occupancy was found to have both oxygens less than 3 Å away from H11A on the amino group of *p*ABA, while the NMe molecule was found to be rotated in the 46% occupancy with O23B found to be 4.8 Å away from H11A

It was observed in the PXRD patterns of the crystals produced from the different solvent mixtures that some peaks were found to shift nonsystematically in 2θ from sample to sample. This was attributed to the disorder of the NMe in the structure, whereby the NMe could occupy the different atomic positions identified from the single crystal structure, or even a mixture of the two (full details in Supporting Information).

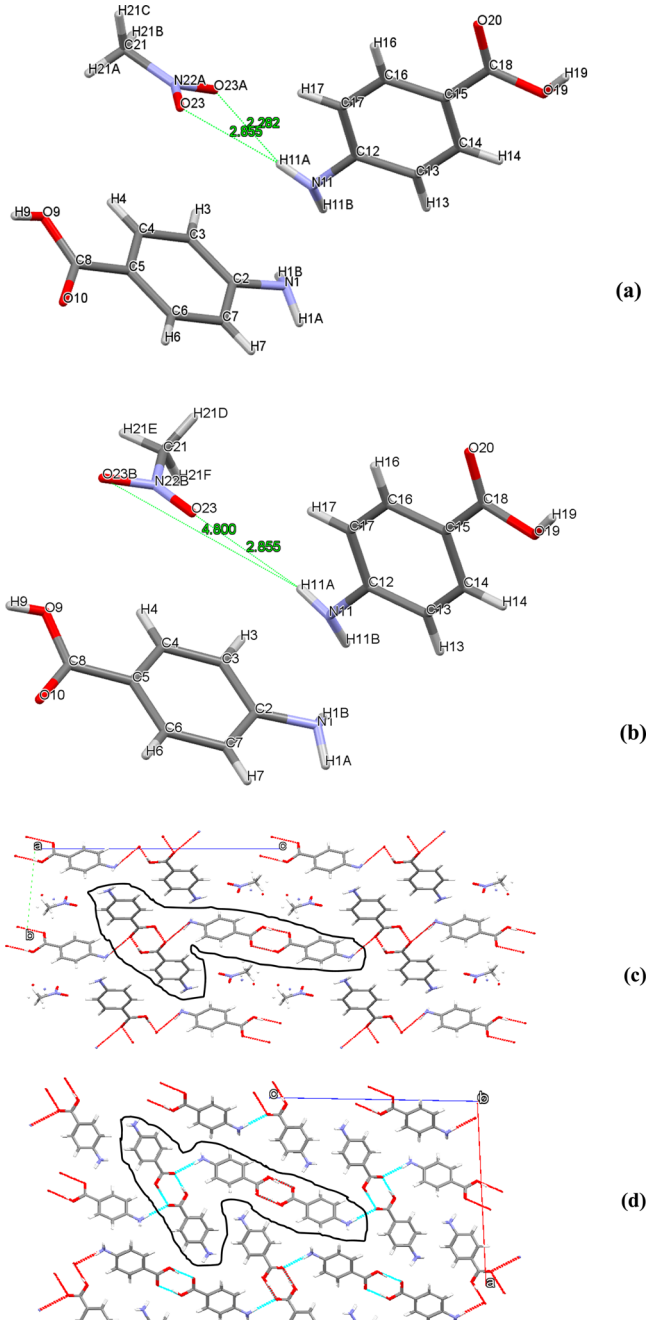

Figure 4. (a) Asymmetric unit of occupancy 1 (54%); (b) asymmetric unit of occupancy 2 (46%); (c) packing of the NMe solvate structure in the *yz* plane, black line identifying the tetramer common to the α-*p*ABA structure and solvate structure; (d) packing of the α-*p*ABA structure in the *xz* plane, black line identifying the tetramer common to the α-*p*ABA structure and solvate structure.

The black lines in Figure 4c,d highlight the existence of essentially identical H-bonded tetramers, (two acid dimers linked by an NH···O hydrogen bond), which exist in both the solvate and α-*p*ABA structure. This would suggest that, analogous to the α-structure, the OH···O H-bonding dimers play a significant role in stabilizing the crystal structure of the solvate. The orientations of the two carboxylic acid H-bonding dimers within the two crystal structures are compared in Figure 5.

DOI: 10.1021/acs.cgd.7b00425
Cryst. Growth Des. 2017, 17, 4151−4161

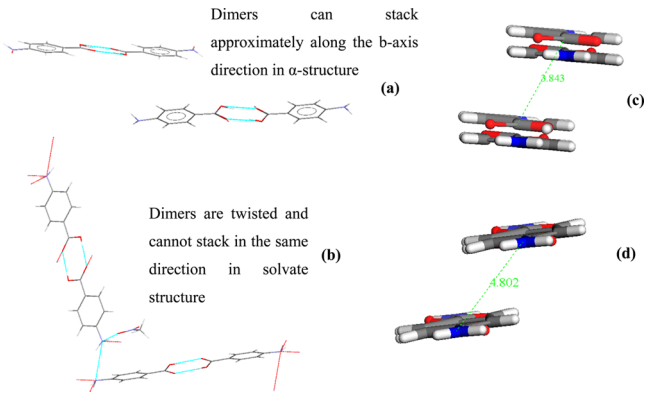

Figure 5. (a) Orientation of the two independent carboxylic H-bonding dimers within the *α*-*p*ABA structure; (b) orientation of the two independent carboxylic acid H-bonding dimers and the NMe molecule within the NMe solvate structure; (c) the stacking of the carboxylic acid dimers in *α*-*p*ABA; (d) stacking of the carboxylic acid *p*ABA dimers in the NMe solvate structure.

Figure 5a shows how the two independent acid dimers pack with the ring structures approximately pointing in the same direction, allowing for efficient close stacking of the dimers through their ring structures along the *b*-axis.[17,49] Comparing (c) and (d), it was found that the stacking of the *p*ABA dimers in the solvate structure ((d)) was far more offset from each other than in the pure *α*-*p*ABA structure ((c)), and the measured distance between two adjacent carbonyl carbons was found to be approximately 1 Å greater in the solvate structure. It can also be observed that the stacking interactions in the *α*-structure form in a continuous and unbroken chain, approximately in the direction of the *b*-axis. In comparison, the stacking of the rings of *p*ABA in the NMe solvate were found to be isolated pairwise interactions, rather than an extended chain of $\pi-\pi$ stacking.

The *b*-axis of the solvate structure was found to lengthen in comparison to the *α*-*p*ABA structure. Figure 4d shows that the NMe molecule is situated between the rings of two *p*ABA molecules, hence forcing the extension along the *b*-axis. In the *α*-*p*ABA structure, both dimers are approximately in the same plane (Figure 5a), and the hydrogen bonds are directed approximately in the A and C directions; hence they are approximately the same length. In the solvate structure, the twisting of the dimers to accommodate the NMe molecule has resulted in the dimers no longer being in the same plane running along the *a*-axis, and hence the *a*-axis has reduced in length (Figure 4c,d).

The calculated strength of the intermolecular interactions (synthons) found within the NMe solvate is shown in Table 2, along with visualization of the pairwise interactions.

The lattice energy calculated for the solvate structure was found to be almost 7 kcal/mol less than the lattice energy calculated for *α*-*p*ABA. Synthons A, B, and C were found to be structurally similar to the strongest synthons found in a study of the *α*-*p*ABA crystal structure;[17] however, they were in general

Table 2. Strongest Synthons Calculated from the Bulk Structure of the NMe Solvate Structure and Compared to the Strongest Synthons from the *α*-*p*ABA Structure[a]

Lattice Energy (kcal/mol)	
Nme Solvate	***α-pABA***
-17.59	*-24.45*
Synthon strengths (kcal/mol)	
A solv: -4.35	*Aα:* -5.67
B solv: -2.09	*Bα:* -2.68
C solv: -2.07	*Cα:* -2.27
D solv: -1.77	*Dα:* -1.21
E solv: -1.63	*Eα:* -0.95
F solv: -1.53	*Fα:* -1.13

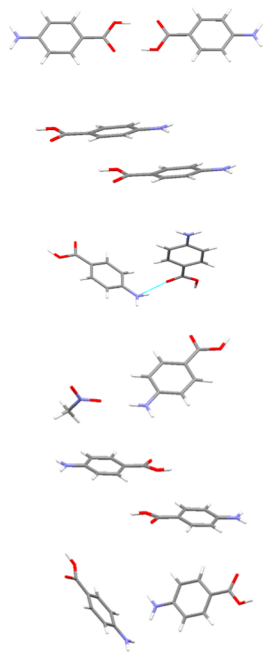

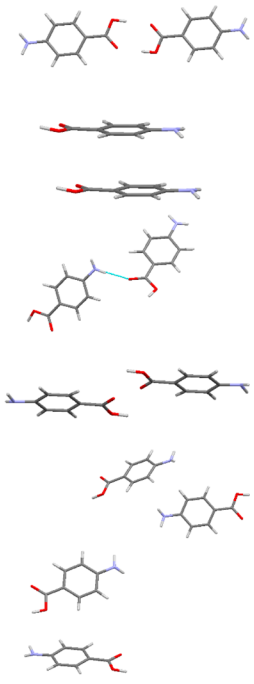

[a]Synthons visualized either side of the table for each structure.

DOI: 10.1021/acs.cgd.7b00425
Cryst. Growth Des. 2017, 17, 4151−4161

calculated to be weaker in the NMe solvate structure when compared to their counterparts in the α-*p*ABA structure.[17] The significantly reduced calculated lattice energy, weaker synthons, and decrease in packing density (Table S2) are consistent with a metastable structure, which correlates to the crystallization data in Section 3.3. Some extra hydrogen bonding interactions were also identified, an NH···O H-bond between the *p*ABA and NMe molecules and an NH···N H-bond between the *p*ABA molecules, which was not found to be present in the α−*p*ABA structure.[17] The presence of the extra hydrogen bonds probably somewhat compensates for the general weaker intermolecular synthonic structure, hence stabilizing the crystal structure.

3.5. Crystal Morphologies from Mixed Solvents. Figure 6 shows images of the crystals produced from the cooling crystallization experiments.

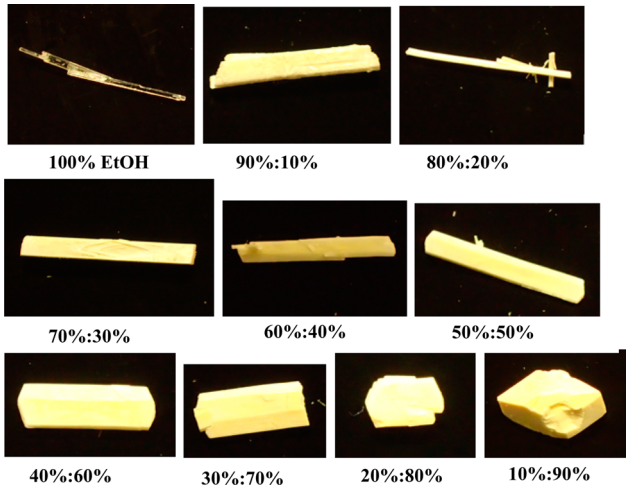

Figure 6. Images of *p*ABA crystallized at S = 1.1 at 10 °C from pure EtOH up to 90:10 NMe/EtOH ratio.

Figure 6 shows that the crystals produced from solutions with increasing NMe content were found to decrease in aspect ratio and become more opaque. Table 1 indicated that the crystals produced from solutions with above 60% NMe content were pure α-*p*ABA, therefore suggesting that the increasing NMe content reduces the aspect ratio of pure α-*p*ABA crystals. Figure 6 also showed that the crystals became more faceted and have smoother surfaces with increasing NMe content. Previous studies suggested that the capping faces which terminate the *b*-axis of α-*p*ABA grow by a rough interfacial growth mechanism from ethanol[74] and that they are often not well formed upon solution crystallization.[49] Therefore, addition of NMe to the solutions appears to stabilize the interface and encourage slower, stable growth of the α-*p*ABA capping faces.

3.6. Rationalization of the Morphological and Structural Data through Solute/Solvent Interaction Modeling. The acid dimer is present in both the α-*p*ABA structure and the solvate structure; therefore the binding of NMe and EtOH was compared using the systematic search shown in Figure 7.

Figure 7a shows that the EtOH molecules were found to prefer to bind to the COOH and NH_2 groups, while the NMe molecules were found to prefer to bind to the NH_2 group and the phenyl ring. This correlates to the orientation of the NMe molecule found within the solvate structure (Figure 4). This observation may be related to the maximum observed in the solubility dependence of *p*ABA on NMe content. This would imply that at a level of 10% NMe in EtOH both the phenyl ring and the carboxylic acid group of *p*ABA experience their maximum solvation.

Figure 7b revealed that the vdW interactions had a relatively small contribution to the binding energy for the EtOH molecule. However, after the addition of a fifth NMe molecule, the vdW contribution to the energy started to increase strongly, consistent with the NMe molecule having a stronger interaction with the phenyl ring. This is supported by Figure 7c, which shows that the systematic search suggested that, in its most favorable position, the NMe molecule prefers to lie across the phenyl ring at the capping face of α-*p*ABA, while EtOH adopts a more orthogonal orientation in order to bind most strongly to the COOH group.

It is interesting to comment that, as well as nitromethane, solvate structures have been produced from acetone and dioxane.[75] In contrast, though there have been extensive studies of the crystallization of *p*ABA from polar protic solvents, such as water and ethanol, no solvate structures have been found and α-*p*ABA often crystallizes instead.[45−47,52,76] This observation could correlate with the fact that EtOH, which is a polar and protic solvent, was found to prefer to strongly interact with the COOH group of *p*ABA. The COOH group forms several strong interactions with other *p*ABA molecules in the α-*p*ABA structure, implying that there is probably not much space around this group. In contrast, the NH_2 and phenyl ring groups probably have a greater amount of space around them in the structure, and the NMe molecule is found to have a greater propensity to interact with those groups. Indeed, the NMe molecule is found to be interacting primarily with the NH_2 group in the solvate structure. Hence, this implies that the space around functional groups, along with the solvent/solute interactions with respect to these functional groups, has a strong influence on the propensity of a particular solvent to produce a solvated crystalline form.

We also suggest that the solute/solvent interactions in the crystal structure and calculated from the molecular and surface systematic searches have implications with respect to the changes in crystal morphology observed in Section 3.5. It has been observed that at the capping surface of α−*p*ABA, the *p*ABA molecules integrate into the surface by forming π−π stacking interactions between the phenyl ring structures.[17] Therefore, the observation that the NMe molecule has a greater propensity to interact with the phenyl ring, in comparison with ethanol, could imply that the presence of NMe results in the observed reduction of the aspect ratio of crystals produced from solutions of increasing NMe concentration. The surface search results shown in Figure 7c suggest that, at the capping face, the binding of the NMe could potentially hinder the formation of the chain of π−π stacking interactions that are thought to strongly influence the needle-like morphology of α-*p*ABA.[16−18,49] This is supported by the observation that such chains of close stacking phenyl rings in the *p*ABA molecules, observed in the α-*p*ABA structure, were found to be absent in the solvate.

4. CONCLUSIONS

This study has demonstrated for the first time how a combined use of the CSD, crystal structure analysis, and molecular and crystal surface modeling of the solute−solvent interactions can provide an insight into the crystalline form and morphology produced from the different solvent mixtures. The calculated

DOI: 10.1021/acs.cgd.7b00425
Cryst. Growth Des. 2017, 17, 4151−4161

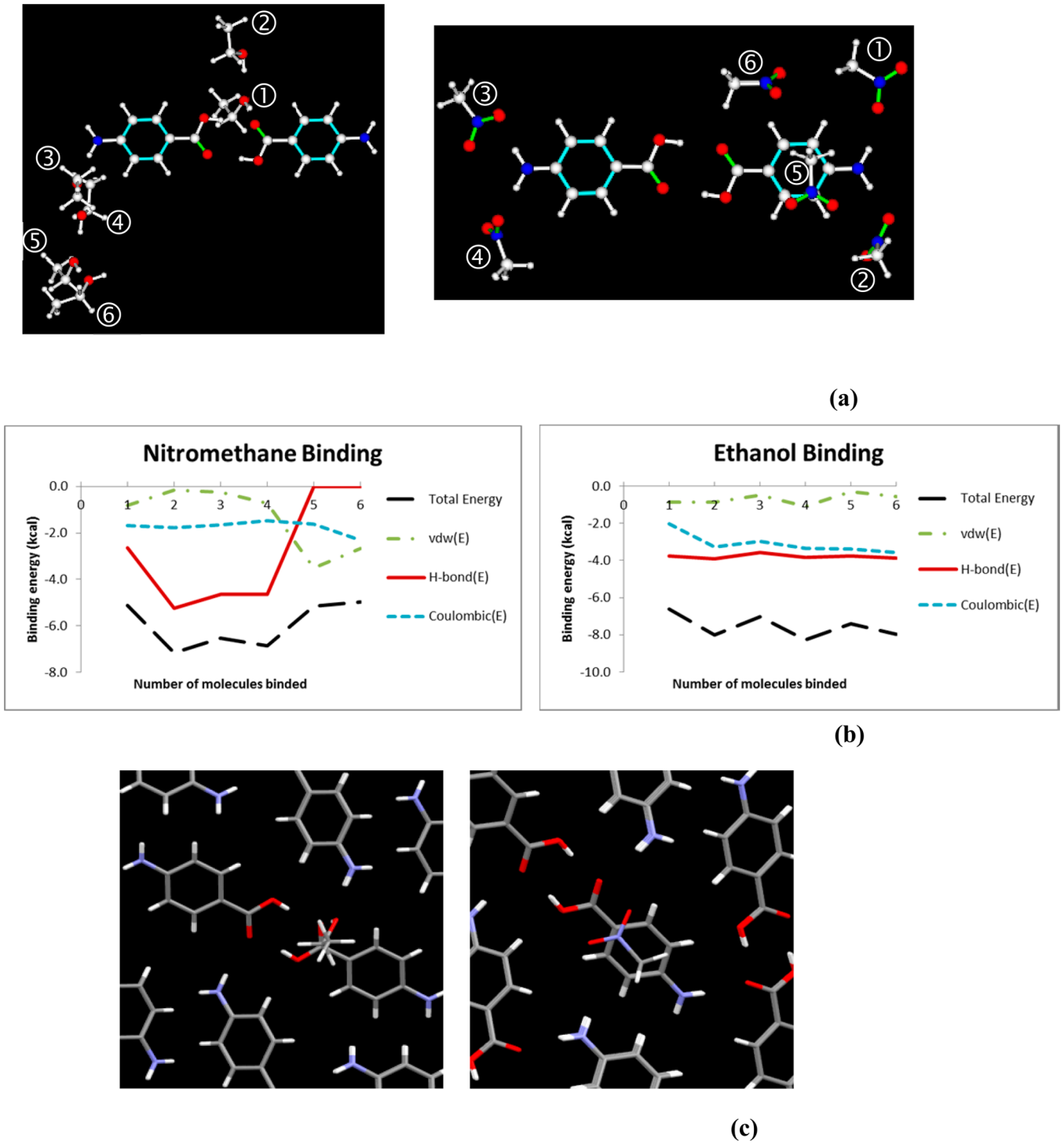

Figure 7. (a) Comparison of the sequential systematic searching of six molecules of ethanol (left) and nitromethane (right); (b) energetic contributions to the sequential molecular binding calculated by the systematic search for ethanol (left) and nitromethane (right); (c) most favored orientation for a probe molecule of ethanol (left) and nitromethane (right) at the (0 1 $\bar{1}$) surface of the α-form of *p*ABA.

propensity of NMe to interact more strongly with the NH_2 and phenyl ring groups, in comparison to a polar protic solvent like EtOH which was calculated to prefer to interact with the COOH group, probably resulted in the formation of the solvate structure, as there was space around the NH_2 group for the NMe molecule to be accommodated.

The observed disorder of the NMe molecules in the solvate crystal structure accounted for the shifting of the peaks in the PXRD, suggesting that the solvate structure could occupy different occupancies when crystallized from solution. This correlated well to the calculated weaker synthonic interactions in the solvate structure, in comparison to the α-structure, along with the observation that α-*p*ABA dominated the crystallization from solutions with >60% NMe content, due to the increased crystallization time.

The greater propensity of the NMe molecule to interact strongly with the phenyl ring group of *p*ABA, along with the observed disruption in the $\pi-\pi$ stacking interactions in the

DOI: 10.1021/acs.cgd.7b00425
Cryst. Growth Des. 2017, 17, 4151−4161

solvate structure, has been correlated to the decrease in aspect ratio of crystals produced from solutions with increasing NMe content. Since the $\pi-\pi$ stacking interactions dominate the growth along the long axis of the needle, the presence of NMe indicates its disruption to these interactions, hence slowing down the growth along the long axis of the needle, producing the observed isotropic morphologies.

This work demonstrates how molecular and crystallographic modeling tools can be combined with in-depth particle analysis to explain the changes in physical properties of a crystalline material. This work can assist in the ongoing efforts to improve the digital design of crystallization processes from solution, in relation to assisting the cleaner and more efficient manufacture of pharmaceutical and fine chemical particulate products.

■ ASSOCIATED CONTENT

Supporting Information

The Supporting Information is available free of charge on the ACS Publications website at DOI: 10.1021/acs.cgd.7b00425.

S1: Overlaying of Molecular Structures. S2: Raw solubility data for all solution compositions. S3: Crystallography and Conformational Analysis. S4: Raw PXRD data from crystals produced from mixed EtOH:NMe solutions. S5: Rietveld analysis of the different occupancies for the NMe solvate structure (PDF)

Accession Codes

CCDC 1539150 contains the supplementary crystallographic data for this paper. These data can be obtained free of charge via www.ccdc.cam.ac.uk/data_request/cif, or by emailing data_request@ccdc.cam.ac.uk, or by contacting The Cambridge Crystallographic Data Centre, 12 Union Road, Cambridge CB2 1EZ, UK; fax: +44 1223 336033.

■ AUTHOR INFORMATION

Corresponding Author

*E-mail: i.rosbottom@leeds.ac.uk.

ORCID

I. Rosbottom: 0000-0001-6342-3973

Present Address

#The Cambridge Crystallographic Data Centre, 12 Union Road, Cambridge CB2 1EZ, UK.

Notes

The authors declare no competing financial interest.

Raw data for this article may be accessed at https://doi.org/10.5518/223.

■ ACKNOWLEDGMENTS

We are grateful to the EPSRC for the support of crystallization research at Leeds and Manchester through the award of a Critical Mass grant "Molecules, Clusters and Crystals" (EP/I014446/1), which supported the Ph.D. studies of two of us (I.R.[77] and T.D.T.[78]). We also gratefully acknowledge the support of the Advanced Manufacturing Supply Chain Initiative through the funding of the "Advanced Digital Design of Pharmaceutical Therapeutics" (Grant No. 14060) project in terms of supporting pharmaceutical crystallization and modelling research at Leeds. We would also like to thank Dr. Christopher Pask (School of Chemistry, University of Leeds) for helpful discussions on the nature of disorder in the NMe solvate structure.

■ GLOSSARY

H-bond, hydrogen bonding
vdW, van der Waals
XRD, X-ray diffraction
PXRD, powder X-ray diffraction
synthons, pairwise intermolecular interactions
slice energy, energy of intermolecular interactions found within one *d*-spacing on the (*hkl*) crystallographic plane
attachment energy, energy of intermolecular interactions formed when a slice one *d*-spacing thick is added to a surface defined by (*hkl*) plane
d-spacing, interatomic plane separation

List of Symbols

ΔH_{fus}, enthalpy of fusion
E_{cr}, lattice energy
E_{sl}^{hkl}, slice energy per surface *hkl*
E_{att}^{hkl}, attachment energy per surface *hkl*
Å, angstroms
R, gas constant
T, absolute temperature
T_m, melting temperature
ΔH_{diss}, enthalpy of dissolution
ΔS_{diss}, entropy of dissolution

■ REFERENCES

(1) Nangia, A.; Desiraju, G. Pseudopolymorphism: occurrences of hydrogen bonding organic solvents in molecular crystals. *Chem. Commun.* **1999**, *7*, 605−606.

(2) Mukherjee, A.; Grobelny, P.; Thakur, T. S.; Desiraju, G. R. Polymorphs, Pseudopolymorphs, and Co-Crystals of Orcinol: Exploring the Structural Landscape with High Throughput Crystallography. *Cryst. Growth Des.* **2011**, *11* (6), 2637−2653.

(3) Bajpai, A.; Scott, H. S.; Pham, T.; Chen, K.-J.; Space, B.; Lusi, M.; Perry, M. L.; Zaworotko, M. J. Towards an understanding of the propensity for crystalline hydrate formation by molecular compounds. *IUCrJ* **2016**, *3* (6), 430−439.

(4) Loschen, C.; Klamt, A. Computational Screening of Drug Solvates. *Pharm. Res.* **2016**, *33* (11), 2794−2804.

(5) Campeta, A. M.; Chekal, B. P.; Abramov, Y. A.; Meenan, P. A.; Henson, M. J.; Shi, B.; Singer, R. A.; Horspool, K. R. Development of a Targeted Polymorph Screening Approach for a Complex Polymorphic and Highly Solvating API. *J. Pharm. Sci.* **2010**, *99* (9), 3874−3886.

(6) Roberts, K. J.; Sherwood, J. N.; Yoon, C. S.; Docherty, R. Understanding the Solvent-Induced Habit Modification of Benzophenone in Terms of Molecular Recognition at the Crystal/Solution Interface. *Chem. Mater.* **1994**, *6* (8), 1099−1102.

(7) ter Horst, J. H.; Geertman, R. M.; van Rosmalen, G. M. The effect of solvent on crystal morphology. *J. Cryst. Growth* **2001**, *230* (1−2), 277−284.

(8) Hammond, R. B.; Pencheva, K.; Ramachandran, V.; Roberts, K. J. Application of grid-based molecular methods for modeling solvent-dependent crystal growth morphology: Aspirin crystallized from aqueous ethanolic solution. *Cryst. Growth Des.* **2007**, *7* (9), 1571−1574.

(9) Chen, J.; Trout, B. L. Computer-Aided Solvent Selection for Improving the Morphology of Needle-like Crystals: A Case Study of 2,6-Dihydroxybenzoic Acid. *Cryst. Growth Des.* **2010**, *10* (10), 4379−4388.

(10) Hod, I.; Mastai, Y.; Medina, D. D. Effect of solvents on the growth morphology of dl-alanine crystals. *CrystEngComm* **2011**, *13* (2), 502−509.

(11) Li Destri, G.; Marrazzo, A.; Rescifina, A.; Punzo, F. How Molecular Interactions Affect Crystal Morphology: The Case of Haloperidol. *J. Pharm. Sci.* **2011**, *100* (11), 4896−4906.

(12) Punzo, F. Unveiling the role of molecular interactions in crystal morphology prediction. *J. Mol. Struct.* **2013**, *1032* (0), 147−154.

DOI: 10.1021/acs.cgd.7b00425
Cryst. Growth Des. 2017, 17, 4151−4161

(13) Singh, M. K.; Banerjee, A. Role of Solvent and External Growth Environments to Determine Growth Morphology of Molecular Crystals. *Cryst. Growth Des.* **2013**, *13* (6), 2413−2425.
(14) McCrone, W., Polymorphism. In *Physics and Chemistry of the Organic Solid State*; Fox, D.; Labes, M. M.; Weissberger, A., Eds.; Interscience: New York, 1965; Vol. *11*.
(15) MacLeod, C. S.; Muller, F. L. On the Fracture of Pharmaceutical Needle-Shaped Crystals during Pressure Filtration: Case Studies and Mechanistic Understanding. *Org. Process Res. Dev.* **2012**, *16* (3), 425−434.
(16) McArdle, P.; Hu, Y.; Lyons, A.; Dark, R. Predicting and understanding crystal morphology: the morphology of benzoic acid and the polymorphs of sulfathiazole. *CrystEngComm* **2010**, *12* (10), 3119−3125.
(17) Rosbottom, I.; Roberts, K. J.; Docherty, R. The solid state, surface and morphological properties of p-aminobenzoic acid in terms of the strength and directionality of its intermolecular synthons. *CrystEngComm* **2015**, *17* (30), 5768−5788.
(18) Walshe, N.; Crushell, M.; Karpinska, J.; Erxleben, A.; McArdle, P. Anisotropic Crystal Growth in Flat and Nonflat Systems: The Important Influence of van der Waals Contact Molecular Stacking on Crystal Growth and Dissolution. *Cryst. Growth Des.* **2015**, *15* (7), 3235−3248.
(19) Aaltonen, J.; Allesø, M.; Mirza, S.; Koradia, V.; Gordon, K. C.; Rantanen, J. Solid form screening − A review. *Eur. J. Pharm. Biopharm.* **2009**, *71* (1), 23−37.
(20) Bauer, J.; Spanton, S.; Henry, R.; Quick, J.; Dziki, W.; Porter, W.; Morris, J. Ritonavir: An Extraordinary Example of Conformational Polymorphism. *Pharm. Res.* **2001**, *18* (6), 859−866.
(21) Walker, E. M.; Roberts, K. J.; Maginn, S. J. A Molecular Dynamics Study of Solvent and Impurity Interaction on the Crystal Habit Surfaces of ε-Caprolactam. *Langmuir* **1998**, *14* (19), 5620−5630.
(22) Clydesdale, G.; Hammond, R. B.; Roberts, K. J. Molecular Modeling of Bulk Impurity Segregation and Impurity-Mediated Crystal Habit Modification of Naphthalene and Phenanthrene in the Presence of Heteroimpurity Species. *J. Phys. Chem. B* **2003**, *107* (20), 4826−4833.
(23) Kwokal, A.; Nguyen, T. T. H.; Roberts, K. J. Polymorph-Directing Seeding of Entacapone Crystallization in Aqueous/Acetone Solution Using a Self-Assembled Molecular Layer on Au (100). *Cryst. Growth Des.* **2009**, *9* (10), 4324−4334.
(24) Nguyen, T. T. H.; Hammond, R. B.; Roberts, K. J.; Marziano, I.; Nichols, G. Precision measurement of the growth rate and mechanism of ibuprofen {001} and {011} as a function of crystallization environment. *CrystEngComm* **2014**, *16* (21), 4568−4586.
(25) Toroz, D.; Rosbottom, I.; Turner, T. D.; Corzo, D. M. C.; Hammond, R. B.; Lai, X.; Roberts, K. J. Towards an understanding of the nucleation of alpha-para amino benzoic acid from ethanolic solutions: a multi-scale approach. *Faraday Discuss.* **2015**, *179* (0), 79−114.
(26) Li, J.; Tilbury, C. J.; Joswiak, M. N.; Peters, B.; Doherty, M. F. Rate Expressions for Kink Attachment and Detachment During Crystal Growth. *Cryst. Growth Des.* **2016**, *16* (6), 3313−3322.
(27) Roberts, K. J.; Hammond, R. B.; Ramachandran, V.; Docherty, R., Synthonic engineering: from molecular and crystallographic structure to the rational design of pharmaceutical solid dosage forms. In *Computational Approaches in Pharmaceutical Solid State Chemistry*; Abramov, Y., Ed. Wiley: New Jersey, USA, 2016.
(28) Tilbury, C. J.; Green, D. A.; Marshall, W. J.; Doherty, M. F. Predicting the Effect of Solvent on the Crystal Habit of Small Organic Molecules. *Cryst. Growth Des.* **2016**, *16* (5), 2590−2604.
(29) McArdle, P. Oscail, a program package for small-molecule single-crystal crystallography with crystal morphology prediction and molecular modelling. *J. Appl. Crystallogr.* **2017**, *50* (1), 320−326.
(30) Gron, H.; Borissova, A.; Roberts, K. J. In-Process ATR-FTIR Spectroscopy for Closed-Loop Supersaturation Control of a Batch Crystallizer Producing Monosodium Glutamate Crystals of Defined Size. *Ind. Eng. Chem. Res.* **2003**, *42* (1), 198−206.
(31) Ma, C. Y.; Wang, X. Z. Model identification of crystal facet growth kinetics in morphological population balance modeling of l-glutamic acid crystallization and experimental validation. *Chem. Eng. Sci.* **2012**, *70*, 22−30.
(32) Duffy, D.; Barrett, M.; Glennon, B. Novel, Calibration-Free Strategies for Supersaturation Control in Antisolvent Crystallization Processes. *Cryst. Growth Des.* **2013**, *13* (8), 3321−3332.
(33) Constance, E. N.; Mohammed, M.; Mojibola, A.; Egiefameh, M.; Daodu, O.; Clement, T.; Ogundolie, T.; Nwawulu, C.; Aslan, K. Effect of additives on the crystal morphology of amino acids: A theoretical and experimental study. *J. Phys. Chem. C* **2016**, *120* (27), 14749−14757.
(34) Flaten, E. M.; Seiersten, M.; Andreassen, J. P. Polymorphism and morphology of calcium carbonate precipitated in mixed solvents of ethylene glycol and water. *J. Cryst. Growth* **2009**, *311* (13), 3533−3538.
(35) Zhang, L.; Yue, L. H.; Wang, F.; Wang, Q. Divisive effect of alcohol-water mixed solvents on growth morphology of calcium carbonate crystals. *J. Phys. Chem. B* **2008**, *112* (34), 10668−10674.
(36) Clydesdale, G.; Roberts, K. J.; Docherty, R. Modelling the morphology of molecular crystals in the presence of disruptive tailor-made additives. *J. Cryst. Growth* **1994**, *135* (1), 331−340.
(37) Clydesdale, G.; Roberts, K. J.; Lewtas, K.; Docherty, R. Modelling the morphology of molecular crystals in the presence of blocking tailor-made additives. *J. Cryst. Growth* **1994**, *141* (3−4), 443−450.
(38) Kuvadia, Z. B.; Doherty, M. F. Effect of Structurally Similar Additives on Crystal Habit of Organic Molecular Crystals at Low Supersaturation. *Cryst. Growth Des.* **2013**, *13* (4), 1412−1428.
(39) Lovette, M. A.; Doherty, M. F. Needle-Shaped Crystals: Causality and Solvent Selection Guidance Based on Periodic Bond Chains. *Cryst. Growth Des.* **2013**, *13* (8), 3341−3352.
(40) Vinodhini, K.; Srinivasan, K. The role of a mixture of DMSO: water in the crystallization of alpha-lactose monohydrate (alpha-LM) single crystals with desired morphology. *CrystEngComm* **2015**, *17* (33), 6376−6383.
(41) Cook, J. L.; Hunter, C. A.; Low, C. M. R.; Perez-Velasco, A.; Vinter, J. G. Preferential Solvation and Htdrogen Bonding in Mixed Solvents. *Angew. Chem., Int. Ed.* **2008**, *47*, 6275−7277.
(42) Prausnitz, J. M. *Molecular Thermodynamics of Fluid-Phase Equilibria*; Prentice-Hall, 1969.
(43) Roberts, K. J.; Hammond, R. B.; Ramachandran, V.; Docherty, R., Synthonic engineering: from molecular and crystallographic structure to the rational design of pharmaceutical solid dosage forms. In *Computational Approaches in Pharmaceutical Solid State Chemistry*; Abramov, Y. A., Ed.; Wiley: New Jersey, USA, 2016.
(44) Moldovan, A. A.; Rosbottom, I.; Ramachandran, V.; Pask, C. M.; Olomukhoro, O.; Roberts, K. J., Crystallographic Structure, Intermolecular Packing Energetics, Crystal Morphology and Surface Chemistry of Salmeterol Xinafoate (Form I). *J. Pharm. Sci.* **2017***106*, (3), 882−891.10.1016/j.xphs.2016.11.016
(45) Svard, M.; Nordstrom, F. L.; Hoffmann, E.-M.; Aziz, B.; Rasmuson, A. C. Thermodynamics and nucleation of the enantiotropic compound p-aaminobenzoic acid. *CrystEngComm* **2013**, *15*, 5020.
(46) Hao, H. X.; Barrett, M.; Hu, Y.; Su, W. Y.; Ferguson, S.; Wood, B.; Glennon, B. The Use of in Situ Tools To Monitor the Enantiotropic Transformation of p-Aminobenzoic Acid Polymorphs. *Org. Process Res. Dev.* **2012**, *16* (1), 35−41.
(47) Gracin, S.; Rasmuson, Å. C. Polymorphism and Crystallization of p-Aminobenzoic Acid. *Cryst. Growth Des.* **2004**, *4* (5), 1013−1023.
(48) Black, J. F. B.; Davey, R. J.; Gowers, R. J.; Yeoh, A. Ostwald's rule and enantiotropy: polymorph appearance in the crystallisation of p-aminobenzoic acid. *CrystEngComm* **2015**, *17* (28), 5139−5142.
(49) Sullivan, R. A.; Davey, R. J. Concerning the Crystal Morphologies of the alpha and beta polymorphs of p-aminobenzoic acid. *CrystEngComm* **2015**, *17*, 1015−1023.
(50) Toroz, D.; Rosbottom, I.; Turner, T.; Corzo, D. M. C.; Hammond, R. B.; Lai, X.; Roberts, K. J. Towards An Understanding of

DOI: 10.1021/acs.cgd.7b00425
Cryst. Growth Des. 2017, 17, 4151−4161

the Nucleation of Para Amino Benzoic Acid: A Multi Scale Approach. *Faraday Discuss.* **2015**, *179*, 79−114.
(51) Prausnitz, J. M. *Molecular Thermodynamics of Fluid Phase Equilibria,* 1969.
(52) Turner, T. D.; Corzo, D. M. C.; Toroz, D.; Curtis, A.; Dos Santos, M. M.; Hammond, R. B.; Lai, X.; Roberts, K. J. The influence of solution environment on the nucleation kinetics and crystallisability of para-aminobenzoic acid. *Phys. Chem. Chem. Phys.* **2016**, *18* (39), 27507−27520.
(53) http://www.julabo.com/en.
(54) http://www.panalytical.com/Home.htm.
(55) Cosier, J.; Glazer, A. M. A nitrogen-gas-stream cryostat for general X-ray diffraction studies. *J. Appl. Crystallogr.* **1986**, *19*, 105−107.
(56) *CrysAlisPRO*; Rigaku Oxford Diffraction: England, 2015.
(57) Clark, R. C.; Reid, J. S. The analytical calculation of absorption in multifaceted crystals. *Acta Crystallogr., Sect. A: Found. Crystallogr.* **1995**, *51*, 887−897.
(58) Sheldrick, G. M. SHELXS97, Program for the Solution of Crystal Structures. *Acta Crystallogr., Sect. A: Found. Crystallogr.* **2008**, *64*, 112−122.
(59) Sheldrick, G. M., Crystal structure refinement with SHELXL. *Acta Crystallogr., Sect. C: Struct. Chem.* **2015**.71310.1107/S2053229614024218
(60) Dolomanov, O. V.; Bourhis, L. J.; Gildea, R. J.; Howard, J. A. K.; Puschmann, H. OLEX2: A complete structure solution, refinement and analysis program. *J. Appl. Crystallogr.* **2009**, *42*, 339−341.
(61) Clydesdale, G.; Docherty, R.; Roberts, K. J. HABIT - a program for predicting the morphology of molecular crystals. *Comput. Phys. Commun.* **1991**, *64* (2), 311−328.
(62) Momany, F. A.; Carruthers, L. M.; McGuire, R. F.; Scheraga, H. A. Intermolecular potentials from crystal data. III. Determination of empirical potentials and application to the packing configurations and lattice energies in crystals of hydrocarbons, carboxylic acids, amines, and amides. *J. Phys. Chem.* **1974**, *78* (16), 1595−1620.
(63) Dewar, M. J. S.; Zoebisch, E. G.; Healy, E. F.; Stewart, J. J. P. Development and use of quantum mechanical molecular models. 76. AM1: a new general purpose quantum mechanical molecular model. *J. Am. Chem. Soc.* **1985**, *107* (13), 3902−3909.
(64) Stewart, J. J. P. MOSOL, MOPAC for Solid-State Physics. *Quant. Chem. Prog. Exchange* **1985**, *5*, 62−63.
(65) Docherty, R.; Roberts, K. J. Modeling The Morphology Of Molecular-Crystals - Application To Anthracene, Biphenyl And Beta-Succinic Acid. *J. Cryst. Growth* **1988**, *88* (2), 159−168.
(66) Docherty, R.; Clydesdale, G.; Roberts, K. J.; Bennema, P. Application Of Bravais-Friedel-Donnay-Harker, Attachment Energy And Ising-Models To Predicting And Understanding The Morphology Of Molecular-Crystals. *J. Phys. D: Appl. Phys.* **1991**, *24* (2), 89−99.
(67) Roberts, K. J.; Docherty, R.; Bennema, P.; Jetten, L. The Importance Of Considering Growth-Induced Conformational Change In Predicting The Morphology Of Benzophenone. *J. Phys. D: Appl. Phys.* **1993**, *26* (8B), B7−B21.
(68) Clydesdale, G.; Roberts, K. J.; Telfer, G. B.; Saunders, V. R.; Pugh, D.; Jackson, R. A.; Meenan, P. Prediction of the Polar Morphology of Sodium Chlorate Using a Surface-Specific Attachment Energy Model. *J. Phys. Chem. B* **1998**, *102* (36), 7044−7049.
(69) Hammond, R. B.; Ma, C. Y.; Roberts, K. J.; Ghi, P. Y.; Harris, R. K. Application of Systematic Search Methods to Studies of the Structures of Urea-Dihydroxy Benzene Cocrystals. *J. Phys. Chem. B* **2003**, *107* (42), 11820−11826.
(70) Hammond, R. B.; Hashim, R. S.; Ma, C.; Roberts, K. J. Grid-based molecular modeling for pharmaceutical salt screening: Case example of 3,4,6,7,8,9-hexahydro-2H-pyrimido (1,2-a) pyrimidinium acetate. *J. Pharm. Sci.* **2006**, *95* (11), 2361−2372.
(71) Hammond, R. B.; Pencheva, K.; Roberts, K. J. Molecular modeling of crystal-crystal interactions between the alpha- and beta-polymorphic forms of L-glutamic acid using grid-based methods. *Cryst. Growth Des.* **2007**, *7* (5), 875−884.
(72) Hammond, R. B.; Pencheva, K.; Ramachandran, V.; Roberts, K. J. Application of grid-based molecular methods for modeling solvent-dependent crystal growth morphology: Aspirin crystallized from aqueous ethanolic solution. *Cryst. Growth Des.* **2007**, *7* (9), 1571−1574.
(73) Ramachandran, V.; Murnane, D.; Hammond, R. B.; Pickering, J.; Roberts, K. J.; Soufian, M.; Forbes, B.; Jaffari, S.; Martin, G. P.; Collins, E.; Pencheva, K. Formulation Pre-screening of Inhalation Powders Using Computational Atom−Atom Systematic Search Method. *Mol. Pharmaceutics* **2015**, *12* (1), 18−33.
(74) Toroz, D.; Rosbottom, I.; Turner, T. D.; Corzo, D. M. C.; Hammond, R. B.; Lai, X.; Roberts, K. J. Towards an understanding of the nucleation of alpha-para amino benzoic acid from ethanolic solutions: a multi-scale approach. *Faraday Discuss.* **2015**, *179*, 79−114.
(75) Killean, R. C. G.; Tollin, P.; Watson, D. G.; Young, D. W. Twinning in *p*-aminobenzoic acid. *Acta Crystallogr.* **1965**, *19* (3), 482−483.
(76) Sullivan, R. A.; Davey, R. J.; Sadiq, G.; Dent, G.; Back, K. R.; ter Horst, J. H.; Toroz, D.; Hammond, R. B. Revealing the Roles of Desolvation and Molecular Self-Assembly in Crystal Nucleation from Solution: Benzoic and p-Aminobenzoic Acids. *Cryst. Growth Des.* **2014**, *14* (5), 2689−2696.
(77) Rosbottom, I. The Influence of Molecular Interactions and Aggregation on the Polymorphism, Crystal Growth and Morphology of Para Amino Benzoic Acid University of Leeds, Leeds, 2015.
(78) Turner, T. D. *Molecular Self-Assembly, Nucleation Kinetics and Cluster Formation Associated with Solution Crystallisation*; University of Leeds: Leeds, UK, 2015.

DOI: 10.1021/acs.cgd.7b00425
Cryst. Growth Des. 2017, 17, 4151−4161